# Percolative diffusion of a dumbbell interstitial defect on a fcc lattice: Calculation of a percolation threshold with use of a series method

J. L. Bocquet
*Centre d'Études Nucléaires de Saclay, Département d'Etudes du Comportement des Matériaux, Section de Recherches de Métallurgie Physique, 91191 Gif-sur-Yvette Cedex, France*
(Received 2 February 1994; revised manuscript received 25 April 1994)

The analogy between electrical conductivity and matter transport holds only in simple cases, where the point defect which is responsible for the diffusion does not alter the shape of the percolating cluster. In the five variants of a model of matter transport by a dumbbell interstitial defect mechanism in fcc alloys, the point defect migrates on a sublattice of coordinance 8 and has only two jump frequencies at its disposal. When the disparity between these frequencies tends to infinity, a percolative regime of diffusion is observed, but the critical threshold arising in the diffusion problem can be identified with a standard percolation one only under restrictive conditions. The present paper evaluates the site percolation threshold $p_c$ corresponding to one of the five variants by the usual series method. Extensive computer enumeration yields perimeter polynomials for clusters containing up to 14 sites. A classical analysis by Dlog-Padé approximants to the first two moments of the cluster density function $n(s)$ yields the two critical exponents $\beta(p_c)$ and $\gamma(p_c)$ associated to the percolation probability and the mean cluster size, respectively, as functions of the (unknown) threshold $p_c$. It is shown further that, using the higher-order moments of the cluster density function $n(s)$, a very tight range for $p_c$ can be proposed $(0.2775 < p_c < 0.2782)$, and that the corresponding values $\beta(p_c)$ and $\gamma(p_c)$ are in close agreement with the recent and most commonly adopted values for both of these exponents.

## I. INTRODUCTION

The approach for the electrical conductivity of an inhomogeneous medium in terms of percolation has been illustrated and worked out in various ways during the last two decades.[1-5] Whereas the first models focused on the problem of hopping conductivity with a continuous distribution of jump probabilities for the charge carriers,[6,7] most of the calculations have tackled the problem of dc and ac conductivity on lattices which were decorated, randomly or not,[8-10] isotropically or not,[11,12] by a binary distribution of conductances, a fraction $p$ of which being either zero (isolating bond) or infinite (superconducting bond): The formulation was later extended to include capacitors[13,14] and even diodes.[15,16] Outside a region centered around some critical threshold $p_c$, the effective conductivity of such lattices can be well approximated by effective-medium approximations,[2,17-19] but its behavior in the vicinity of the threshold obeys scaling laws instead: Most of the preceding quoted studies focused their effort on the determination of the critical exponents rather than on the determination of $p_c$ itself, since only the difference $p - p_c$ is the relevant parameter. Real-space renormalization methods seem now to bridge the gap between both approaches, since they yield both the critical exponents and the value of $p_c$,[20,21] and further, provide also an approximation of the conductivity far from $p_c$, which turns out to be even better than the effective-medium one, at least for simple two-dimensional (2D) lattices.[20]

The problem of mass transport in solids has been recently envisaged with the preceding theories as a starting point.[22,23] Although the formulation is that of a random walk on a lattice, it cannot be straightforwardly taken as a realistic and physical description of diffusion since the analogy between electron and mass transport, although intuitive, is not quite obvious. Indeed, unlike the electronic transport, a severe complication arises in solid-state mass transport, where diffusion is known to be mediated by point defects, which reshuffle permanently the components of the medium among the available lattice sites. In the most simple diffusion models we can think of for random substitutional binary alloys, the point defect is viewed as a random walker which has two jump frequencies at its disposal, the choice between them being dictated by local considerations: In the case of a vacancy mechanism, for instance, the frequency depends on the chemical nature of the atom with which it exchanges;[24,25] for the dumbbell interstitial mechanism, the composition of the defect itself plays a role too,[26,27] as will be recalled in more detail hereafter. The only approaches which take explicitly into account the nature of the point defect and the details of the atomic jump mechanism are effective-medium approximations of the diffusion problem itself. Numerous Monte Carlo simulations have shown that they are quantitatively reasonable, as long as the disparity in the jump frequency is not too large.[28,29] On further consideration, the agreement is all the more surprising as the analytical approach cannot include detailed modifications of the lattice site occupancies operated by the defect migration, whereas the simulation algorithm takes them explicitly into account.

When the disparity of the jump frequencies becomes very large and tends to infinity, the onset of a percolative regime shows up. In the case of the vacancy mechanism, the vacancy will exchange with only one species (say, $B$) while avoiding the other ($A$): Long-range diffusion is possible only if the concentration of the mobile species is

 

above some critical threshold. Below the threshold, the defect is trapped in $B$ clusters of finite size, which are entirely embedded in the immobile ($A$) component; above the threshold, there exists one infinite $B$ cluster spanning over the entire alloy and allowing the long-range migration of the point defect. The agreement between the mean-field model and the numerical simulations deteriorates within a small concentration range around the critical threshold. In the usual case where the vacancy is believed to migrate via first-neighbor jumps, the critical threshold is the site percolation threshold $p_c^s$ (the clusters being defined by a first-neighbor distance criterion on the chosen lattice). The analytical mean-field treatment can only yield an approximate value of the threshold, which turns out to be simply related to a characteristic of the transport mechanism:

$$p_c^s = 1 - f_0 \ , \tag{1}$$

where $f_0$ is the self-diffusion correlation factor by the vacancy mechanism. It is worth noticing that the resulting value is reasonably close to the exact (and well-known) value on several lattices (Table I). The 3D lattice with coordinance 8 mentioned in the table is the object of the present study: In this lattice, the self-diffusion correlation factor has already been determined.[26] It can be checked that the mean-field approximation overestimates the percolation threshold for 3D lattices and underestimates it in 2D, the agreement being closer with an increasing coordination number.

The object of the present paper is the evaluation of a percolation threshold in the case where the point defect is of dumbbell interstitial type and migrates on a sublattice of the parent fcc lattice. The first part recalls the physical origin of the problem, the nature of the critical threshold arising in the diffusion problem, and the conditions under which it can be identified with a percolation threshold evaluated on a suitable lattice. The second part is devoted to the calculation of the percolation threshold by the usual series method together with the critical exponents $\beta$ (associated with the percolation probability) and $\gamma$ (associated with the mean size of the clusters). The last part compares the present result with a former evaluation based on a mean-field formulation of the dumbbell diffusion in concentrated alloys.

TABLE I. Comparison of the site percolation threshold $p_c^s$ and the self-diffusion correlation factor $f_0$ for the vacancy mechanism on several lattices. The 3D lattice of coordinance 8 is the object of the present study and the corresponding value of $p_c^s$ is being determined.

| Lattice | $f_0$ | $1-f_0$ | $p_c^s$ |
|---|---|---|---|
| 1D | 0.0 | 1.0 | 1.0 |
| 2D, hexagonal | 0.333 | 0.666 | 0.700 |
| 2D, square | 0.467 | 0.534 | 0.590 |
| 2D, triangular | 0.560 | 0.440 | 0.500 |
| 3D, diam. | 0.500 | 0.500 | 0.428 |
| 3D, sc | 0.653 | 0.347 | 0.310 |
| 3D, coordinance 8 | 0.689 | 0.311 | unknown |
| 3D, bcc | 0.727 | 0.273 | 0.245 |
| 3D, fcc | 0.781 | 0.219 | 0.198 |

## II. MIGRATION OF THE DUMBBELL DEFECT IN A BINARY fcc ALLOY

### A. Atomistic migration mechanism

In a fcc lattice the interstitial defect, when sufficiently undersized, consists in an extra atom which sits at the center of a regular octahedral cage, the vertices of which are occupied by atoms on substitutional sites. The case of the self-interstitial (produced by irradiation, for instance) does not fit this picture, since the extra atom, which is now of the same size as the surrounding ones, is too big to content itself with the interstitial location of octahedral type. Diffuse x-ray experiments together with numerical simulations agree that this extra atom prefers to share a substitutional lattice site with a neighbor and make up an anisotropic dumbbell-shaped point defect at the expense of a rather large deformation of the surrounding lattice. This dumbbell is dissociated along a $\langle 100 \rangle$ direction and will be denoted by $I_{AA}$; the dissociation distance between the two-constituting atoms, denoted by $2\lambda$, is roughly $0.4 s_0$, where $s_0$ stands for the first-neighbor distance at rest.

The migration mechanism consists of a translation to a nearest-neighbor site together with a $\pi/2$ rotation of the dissociation axis, in such a way as an $x$ dumbbell (dissociated along $\langle 100 \rangle$) on the origin will form a $y$ dumbbell (dissociated along $\langle 010 \rangle$) at $(\pm 1, 1, \pm 1, 0)$, or a $z$ dumbbell (dissociated along $\langle 001 \rangle$) at $(\pm 1, 0, \pm 1)$ with a spacing between (100) planes equal to unity. As shown in Fig. 1, the rear part of the defect (atom 1) comes back on a substitutional site, whereas the front part (atom 2) kicks a neighbor (atom 3) out of its site to build up the new defect. During such a jump, three atoms are moving simultaneously.

It is easy to check that a defect starting from the origin with a given dissociation axis will visit only three of the four simple cubic (sc) sublattices which make up the initial fcc lattice; the last one will be called the forbidden sublattice. The whole set of available sites can be viewed as the vertices of a sc array of octahedra, as depicted in Fig. 2, with a coordinance equal to 8. With such a jump mechanism, a given site is always visited by a defect having the same dissociation axis: As a consequence, a site on which the defect is dissociated along $Ox$ ($Oy$ or $Oz$) will be called an $x$ ($y$ or $z$) site, respectively. In the same

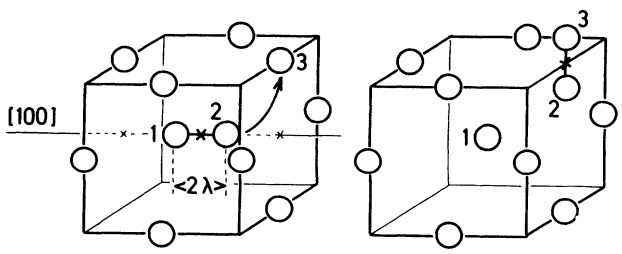


FIG. 1. Atomic mechanism for the migration of the dumbbell interstitial in a fcc lattice. The defect cannot reach any of the four neighbors which are located in its mirror symmetry plane.

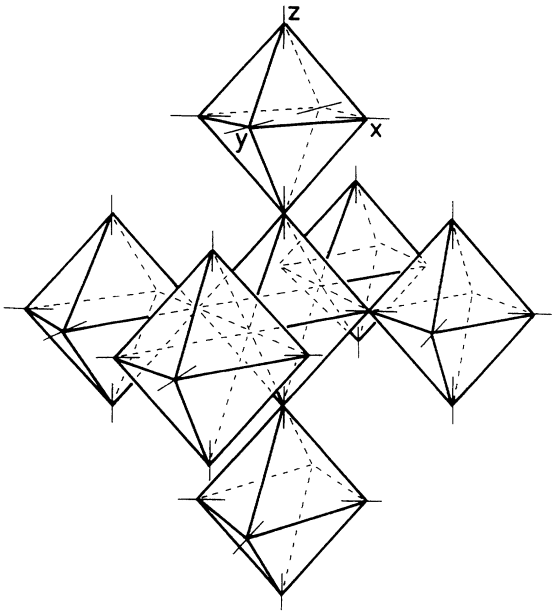


FIG. 2. Lattice available to a defect starting on site labeled $X$ with a dissociation axis along $O_x$ (the short straight line running through each site recalls the dissociation axis of the defect on this site).

way, it can be checked that all the $x$ sites belong to one sc sublattice and that an $x$ site has only $y$ and $z$ neighbors.

In order to describe the migration of such a defect in a binary random alloy $(A,B)$ (atomic concentration $C_A, C_B$), we must foresee all possible events occurring during the displacements, namely, the formation of $I_{AB}$ and $I_{BB}$ type of interstitials, which will unavoidably form as soon as the concentration $C_B$ is no longer negligible. For that purpose, we assume that the jump of a $I_{ij}$ defect toward an atom of type $k$ ($i,j,k = A$ or $B$) will result in the formation of a new interstitial $I_{jk}$, according to the displacements pictured above, the new configuration of the defect being energetically more or less favorable than the preceding one. Knowledge of all the frequencies $W_{ij/k}$ ($i,j,k = A$ or $B$) is sufficient to pin down the rules which master the migration in the alloy. In order to keep the number of arbitrary parameters to a minimum, we make the two simplifying assumptions which follow.

(i) In the actual alloy, the dissociation distance of the $I_{AB}$ and $I_{BB}$ defects will probably differ from its value for $I_{AA}$, since the local deformations around the defect will not be identical. The defect will therefore migrate on a distorted lattice. We assume that the connectivity of the lattice together with the propagation rule for the defect will remain unaltered over the whole concentration range of the solid solution, which is the most important point. The defect jump frequency is further assumed to depend only on the possible variation of the chemical composition of the defect, but not on the atomic local configuration of the alloy.

(ii) Denoting by $E_{ij}$ the formation energy of an $I_{ij}$ defect, the jump frequency $W_{ij/k}$ is given by

$$W_{ij/k} = W_R \min(1, \exp[(E_{ij} - E_{jk})/kT]) \ . \tag{2}$$

In order to reduce the number of unknown parameters, the differences $E_{AA} - E_{BB}$ and $E_{AB} - E_{BB}$, whenever non-null, will take only two opposite values $+\Delta E$ and $-\Delta E$, which are also assumed not to depend on the local configuration of the alloy. As a consequence, each jump frequency which brings no composition change for the defect, or which leads the latter into a configuration of lower energy, will be equated to the more rapid frequency $W_R$. Conversely, each detrapping frequency which brings the defect to a configuration of higher energy will be equated to $W_L$ smaller than $W_R$ according to

$$W_L = W_R/\Theta \ , \tag{3}$$

with

$$\Theta = \exp(|\Delta E|)/kT \ .$$

It is easy to check that these rules comply with the requirements of the detailed balance. All the above assumptions are recorded in a 1D picture (Fig. 3), which synthesizes all the possible variants of a unique underlying model resting on two jump frequencies only: The first three variants are trapping models in which the defect $I_{AA}$ is trapped by the solute $B$, since $E_{AB}$ is lower than $E_{AA}$; the only difference lies in the value for $E_{BB}$ which is lower than, equal to, or higher than $E_{AB}$, and which yields a double trapping (DT), a single trapping (ST), and a single symmetric trapping model (SST), respectively. The fourth variant is a single antitrapping model (SAT), in which $E_{AB}$ is higher than $E_{AA}$ and $E_{BB}$. The last variant is a single delayed trapping model (SDT), in which the pinning of the defect is performed only after it has incorporated two $B$ atoms.

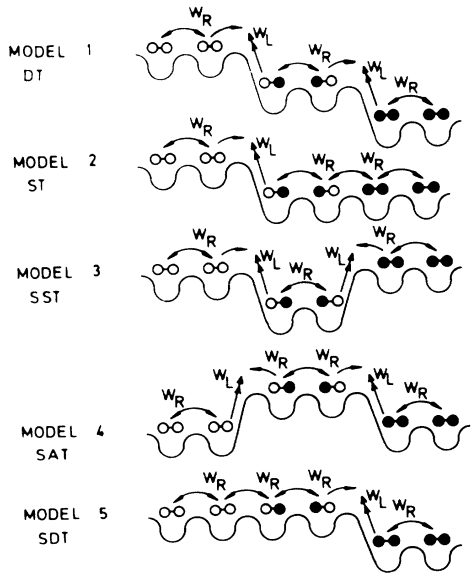


FIG. 3. Schematic 1D picture of the energy barriers to be overcome by a dumbbell interstitial in a binary alloy. Five possible variants of a two frequency model are pictured (DT for double trapping, ST for single trapping, SST for single symmetric trapping, SAT for single antitrapping, and SDT for single delayed trapping).

Like the vacancy case, the assumption that the jump frequency does not depend on the local configuration of the surroundings can be shown to keep the short-range-order parameter to zero: This means that the jump model is consistent with the random assumption for the alloy.

In all the following, we restrict ourselves to the long-time behavior of the defect, which implies that it will use under the form $I_{AA}$, $I_{AB}$, and $I_{BB}$ the proportions of time dictated by the detailed balance equations. Assuming that the total interstitial defect concentration $C_I$ is maintained at a constant value much smaller than the concentrations $C_A$ and $C_B$, and denoting by $P_{ij}$ the proportion of dumbbell $I_{ij}$, the detailed balance equations are

$$P_{AA}C_B W_{AA/B}=P_{BA}C_A W_{BA/A} , \tag{4a}$$

$$P_{AB}C_B W_{AB/B}=P_{BB}C_A W_{BB/A} , \tag{4b}$$

with

$$P_{AA}+P_{AB}+P_{BA}+P_{BB}=1 . \tag{4c}$$

The above three equations can easily be solved for $P_{AA}, P_{AB}=P_{BA}, P_{BB}$ as functions of $\Theta=W_R/W_L$ and $W_{ij/k}$. The four frequencies in Eqs. (4) are equal to $W_R$ or $W_L$, depending on the variant which is chosen according to Fig. 3. The proportions $P_{AB}$ and $P_{BA}$, although numerically equal, are written differently for a possible asymmetry of the model: The jump frequency $W_{BA/A}$ can differ from $W_{AB/A}$ (which is by definition always taken equal to $W_R$).

### B. Onset of the percolative behavior

The onset of the percolative behavior manifests itself when the ratio $\Theta=W_R/W_L$ tends to infinity. In this limit, only the interstitials with nonzero proportion will survive, namely, $I_{BB}$ for variants 1 and 5 ($P_{BB}=1$), $I_{AB}$ and $I_{BB}$ for variant 2 [$P_{AB}=P_{BA}=C_A C_B/(2C_A C_B+C_B^2)$, $P_{BB}=C_B^2/(2C_A C_B+C_B^2)$], $I_{AB}$ for variant 3 ($P_{AB}=P_{BA}=\frac{1}{2}$), and $I_{AA}$ and $I_{BB}$ for variant 4 [$P_{AA}=C_A^2/(C_A^2+C_B^2)$, $P_{BB}=C_B^2/(C_A^2+C_B^2)$]. The behaviors of these variants are markedly different from one another and are briefly reviewed in the following.

#### 1. *Models with only one type of surviving defect*

For variants 1 and 5, the necessary and sufficient condition for the defect $I_{BB}$ to migrate is to have a $B$ atom as a first neighbor. Its long-range diffusivity will be non-null only if there exists an infinite cluster of $B$ atoms spanning through the entire alloy. The critical threshold $p_{c1}$ ($=p_{c5}$) to be determined in this case is clearly the site percolation threshold $p_c^s$ of the lattice depicted in Fig. 2. The value obtained by the mean-field approximation is $p_{c1}=0.280$.[26]

For variant 3, the surviving defect $I_{AB}$ is polarized: The jump is possible toward a first neighbor $B$ if the defect is in the $I_{BA}$ state and toward $A$ if the defect is in the $I_{AB}$ state. But this condition is expressed as a function of the defect composition, which can change at each step, and is not an independent characteristic of the lattice alone. It can be checked that the problem does not reduce to a standard site percolation problem. We could not reduce our problem to a site-correlated problem (similar to "antipercolation" as defined in Ref. 10) or to a polychromatic bond percolation one in the spirit of Ref. 30. The main difficulty is illustrated in Fig. 4 (which is drawn in 2D for sake of simplicity) and resides in the fact that the defect can migrate through a bond in two different ways. The first one changes the site occupancy, and the optimum configuration is a mixed one [Fig. 4(a)]; the second does not, and the optimum configuration is one colored [Fig. 4(b)]. Hence a conflict arises about the condition under which the bond can be declared conducting or not.

It can be understood at this stage why the case of the vacancy mechanism and of variant 1 or 5 of the present interstitial mechanism are so easily reducible to a site percolation problem: In both cases, only one chemical species ($B$) is mobile and mass transport alters neither the occupancies of the lattice sites nor the shape of the percolating cluster since the only effect of the defect migration is to replace a $B$ atom by another one. As a consequence, difficulties will show up whenever the shape of the percolating cluster can be modified by the defect migration: In our problem, it will happen whenever $I_{AB}$ is the (or one of the) surviving type(s) of defect.

The Monte Carlo simulations of the diffusion for higher values of $\Theta$ ($10^4$) suggest that $p_{c3}<p_{c1}$,[27] and the mean-field approximation of the diffusion problem yields a critical threshold $p_{c3}=0.076$.[26]

#### 2. *Models with two types of surviving defects*

For variant 2, the remaining defects $I_{AB}$ and $I_{BB}$ can convert into one another. Both species are mobile as soon as $C_B>p_{c2}$. We could not identify the critical threshold with that of a standard percolation problem for the same reason as above.

Simulations results suggest that $p_{c2}<p_{c3}$,[27] and the mean-field approximation yields $p_{c2}=0.065$.[26] The fact that $p_{c2}<p_{c3}$ can be intuitively justified by the observation that variant 2 can be seen as a superposition of variants 1 and 3. Indeed, the defect can propagate under the form $I_{AB}$, like variant 3, but has the additional possibility to propagate also long paths which are permeable to $I_{BB}$, which was not allowed in variant 3: hence, a lower value for $p_c$.

For variant 4, two types of interstitial dumbbells coexist, but cannot convert into one another unlike the case of

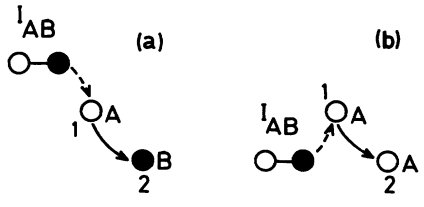


FIG. 4. Two ways of migrating through a bond for the mixed defect $I_{AB}$ of variant 3: (a) jump with occupancy change of site labeled 1 and (b) jump without occupancy change.

variant 2. Each type of defect migrates on a different subset of lattice sites: The long-range migration for $I_{AA}$ ($I_{BB}$) defect takes place in $A$ ($B$) clusters and is submitted to the condition $C_A$ ($C_B$) $>p_{c1}=p_c^s$, respectively. Whereas the model predicts the existence of a critical threshold for each alloy component, the interstitial population, considered as a whole, keeps a non-null mobility over the entire composition range: This last point is confirmed by simulations.[26,27]

The main conclusion of Sec. II B is that the critical threshold $p_{c1}$ is the only one which can be easily identified with that of a standard site percolation one and therefore can be calculated by standard methods as described hereafter. The other thresholds pertain to a new type of percolation problem.

## III. DETERMINATION OF $p_{c1}$ BY THE SERIES METHOD

The concentration $C_B$ is renamed $p$ and the threshold $p_c^s$ is denoted by $p_c$ hereafter.

The determination of $p_c$ rests on the knowledge of the cluster density $n(s)$ evaluated per lattice site, as a function of the size $s$ of the isolated $B$ cluster, that is, entirely surrounded by $A$ atoms:

$$n(s)=p^s D_s(q) , \tag{5a}$$

with

$$q=1-p .$$

The term $p^s$ stands for the presence probability of $s$ atoms on the $s$ sites of the cluster; the polynomial perimeter $D_s(q)$ can be written as

$$D_s(q)=\sum_{i=c_{\min}(s)}^{c_{\max}(s)} d(s,i)q^i . \tag{5b}$$

$d(s,i)$ is the number of clusters of sizes $s$ with a perimeter of $i$ sites; $c_{\min}(s)$ and $c_{\max}(s)$ are the number of lattice sites in the perimeter of the most compact and less dense cluster, respectively. It will be established later that in our case $c_{\min}(s)$ is not a monotonous increasing function of $s$ (Fig. 5), unlike $c_{\max}(s)$ which is equal to $4(s+1)$.

We give in Appendix A the polynomial perimeters for all the clusters of size less than or equal to 14. An automatic counting routine[31,32] reviews all the possible clusters with the correct multiplicity, thanks to a labeling of the available lattice sites in a strictly ascending order. The presence of three different types of sites requires three independent calculations starting with the first atom of the cluster on an $x$ ($y$ or $z$) site, respectively: The average over the three orientations is performed in a subsequent step. Although some rewriting of the program has been performed to speed it up, each calculation required roughly 1300 h CPU time on a HP-730 workstation. The same algorithm, after deleting that part devoted to the analysis of the perimeter, is noticeably faster. We have been able then to count the total number of clusters made of 16 atoms, performing once more three independent runs for the $x$, $y$, and $z$ types of the origin: Each run required 3500 H CPU time of a HP-730 workstation. It is well known that this last enumeration yields one more term in the power-series expansion of the average size $S(p)$,[33] avoiding direct enumeration of the polynomial perimeters for clusters of size $s_{\max}=15$ atoms. In the present problem, we observed that obtaining one more term in the series expansion of $S(p)$ would have required 8.6 times more computation. We report in Table II the number of clusters containing up to 16 sites. After this work had been started, a new and more powerful algorithm was published:[34] The detailed comparison presented in Appendix B shows that we could have gained one more term in the series $S(p)$ with roughly the same computational effort.

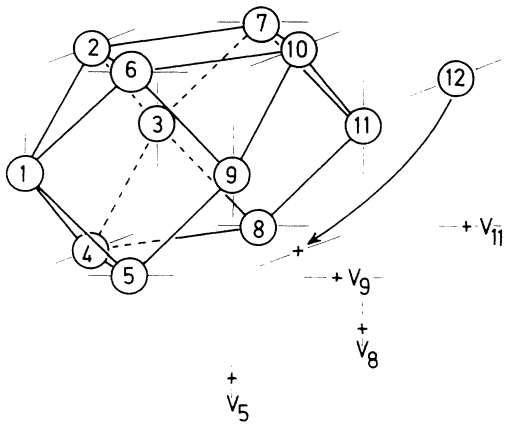


FIG. 5. The perimeter for the most compact cluster made of 11 sites is larger than the perimeter for the corresponding one made of 12 sites. The sites labeled $V_5, V_8, V_9, V_{11}$ are first neighbors of sites 5,8,9,11, respectively, and all of them are first neighbors of the vacant site. Adding the 12th atom on this site occupies a location which was on the perimeter of the preceding cluster, but introduces no new perimeter sites.

The probability that a randomly chosen lattice site is occupied by a $B$ atom is of course equal to $p$; it is made up of two terms $p_{\text{fin}}$ and $p_\infty$, which stand, respectively, for the concentration of $B$ atoms belonging to finite and infinite clusters, respectively:

$$p=p_{\text{fin}}+p_\infty , \tag{6a}$$

with

$$p_\infty=0 \quad \text{for } p<p_c .$$

Last, the concentration of $p_{\text{fin}}$ is nothing but the proportion of lattice sites which are occupied by $B$ atoms involved in finite clusters:

$$p_{\text{fin}}=\sum_0^{s_{\max}} sn(s) . \tag{6b}$$

The threshold is evaluated in two different ways, according to whether $p$ tends to $p_c$ by higher or lower values.

TABLE II. Total number of clusters up to 16 sites (the root of the cluster being on an $x$, $y$, or $z$ site).

| $s$ | Origin $x$ | Origin $y$ | Origin $z$ |
|---|---|---|---|
| 1 | 1 | 1 | 1 |
| 2 | 4 | 4 | 4 |
| 3 | 22 | 22 | 24 |
| 4 | 140 | 140 | 158 |
| 5 | 971 | 972 | 1111 |
| 6 | 7101 | 7117 | 8199 |
| 7 | 53 869 | 54 035 | 62 706 |
| 8 | 420 162 | 421 662 | 492 492 |
| 9 | 3 349 242 | 3 362 182 | 3 948 719 |
| 10 | 27 165 995 | 27 276 130 | 32 188 395 |
| 11 | 223 497 229 | 224 431 081 | 265 955 617 |
| 12 | 1 860 608 738 | 1 868 524 962 | 2 222 256 250 |
| 13 | 15 645 140 550 | 15 712 362 940 | 18 745 545 959 |
| 14 | 132 684 077 789 | 133 256 578 887 | 159 415 759 942 |
| 15 | 1 133 629 985 864 | 1 138 522 789 711 | 1 365 285 138 418 |
| 16 | 9 748 315 489 721 | 9 790 287 997 333 | 11 765 031 921 861 |

### A. Examining the percolation probability $P(p)$ in the high-density domain ($p > p_c$)

In this domain, the probability of having an infinite cluster is unity; the percolation probability is that a fraction $P(p)$ of the solute $B$, which belongs to the infinite cluster and is defined by

$$P(p)=p_\infty/p=1-p_{\text{fin}}/p\ , \tag{7}$$

tends to unity together with $p$ and vanishes at $p_c$ with a critical exponent $\beta$:

$$P(p)=B_1(p-p_c)^\beta,\quad p\to p_c+\ , \tag{8a}$$

or, with respect to the variable $q=1-p$,

$$P(q)=B_1(q_c-q)^\beta,\quad q\to q_c-\ , \tag{8b}$$

with $q_c=1-p_c$. The percolation probability is calculated as a series development in ascending powers of $q$, after an expansion of $p^s$ of relation (5a) as a polynomial with respect to $q=1-p$.

The corresponding coefficients are gathered in the second column of Table III. Apart from the constant term, the order of the first nonvanishing coefficient is equal to the number of first neighbors in the studied lattice, as expected.

The magnitude and sign of the coefficients exhibit an oscillatory behavior with a period of 3. The ratio method applied to each subset of coefficients ($a_{n-3}/a_n$) yields too erratic results to deduce anything reasonable about the value of the threshold.

The analysis by the $D$ log Padé approximant $(l,m)$ consists in reproducing the first terms of $P(q)$ by dividing a polynomial $Q_l$ of degree $l$ by a polynomial $Q_m$ of degree $m$ with $l+m$ less than or equal to the degree of $P(q)$: Then the smallest real positive root $q_c$ of $Q_m$ is looked for and identified with $1-p_c$.

Since the ratio of two polynomials cannot approximate the noninteger divergence of $P(q)$, we are forced to work on the logarithmic derivative $P'(q)/P(q)$ which has a simple pole at $q_c$ together with a residue equal to $\beta$. As a consequence, the series $P(q)$ must be formally derived to yield $P'(q)$, which is then divided term by term by $P(q)$ to obtain the desired $D$ log series.

The term of highest order available in $P(q)$ is equal to the smallest possible number of sites in the perimeter of the cluster with $s_{\max}$ atoms, provided that all the higher-

TABLE III. Coefficients of the series developments for the percolation probability $P(q)$ and for the average cluster size $S(p)$.

| Term of order | Coefficients for $P(q)$ | Coefficients for $S(p)$ |
|---|---|---|
| 0 | 1 | 1 |
| 1 | 0 | 8 |
| 2 | 0 | 40 |
| 3 | 0 | 168 |
| 4 | 0 | 720 |
| 5 | 0 | 2886 |
| 6 | 0 | 11 684 |
| 7 | 0 | 46 536 |
| 8 | −1 | 181 328 |
| 9 | 0 | 699 036 |
| 10 | 0 | 2 750 526 |
| 11 | 0 | 10 404 028 |
| 12 | −8 | 39 801 856 |
| 13 | 8 | 152 038 466 |
| 14 | 0 | 576 712 002 |
| 15 | −32 | 2 161 825 978 |
| 16 | 24 | |
| 17 | 52 | |
| 18 | −196 | |
| 19 | 80 | |
| 20 | 566 | |
| 21 | −1406 | |
| 22 | 252 | |
| 23 | 5264 | |
| 24 | −13 090 | |
| 25 | 8756 | |
| 26 | 31 010 | |
| 27 | −107 232 | |
| 28 | 131 822 | |
| 29 | 98 314 | |

order clusters will have a minimum perimeter strictly larger than that of $s_{max}$. It is shown in Appendix A that this condition is not always fulfilled, but it can be reasonably assumed that this kind of irregularity will occur only when a cluster (or some part of it) will close up the shell around a forbidden site of the parent fcc lattice, which is not the case for the cluster with $s_{max}=16$ sites.

The whole set of the couples $(\beta,pc)$ is copius (120 values) and is shown in Fig. 6. It can be seen that the results gather fairly well around a decreasing curve, as mentioned very often in the literature. But the nature of this curve has never been made explicit. It is remarkable that the whole set of results can be reasonably well represented by a single exponential over five orders of magnitude. It is often argued that the higher-order approximants close to the diagonal ones are the best. Taking due account of the fact that the first term of $P'(q)/P(q)$ is of seventh order, we would expect the best results from the approximants $[l=19\rightarrow16,\ m=9\rightarrow12]$; a careful inspection of our numerical results shows that such approximants yield poles which are very often either complex or wide apart from the expected result, while the more "exotic" [13,15], [15,13], [21,7], and [22,5] approximants are the only ones which give results in the range $0.27<pc<0.28$ where the threshold is expected. In the absence of a practical confirmation of this theoretical recipe, we performed a least-squares fitting of all the results lying in the range (0.25,0.35) which contains more than 75% of the results and which is marked by the boxed area. The fitting expression is found to be

$$\beta(p)=517.7\exp(-25.755p)\ . \tag{9}$$

We know that this route for obtaining the relationship $\beta(p)$ is not the best, since it rests on the development of perimeter polynomials obtained for finite-size clusters below $p_c$, that is, on the counting of large clusters which are less numerous.[35] It will prove, however, to be useful when used in conjunction with the values obtained for the critical exponents associated with the higher-order moments of $n(s)$.

### B. Examining the cluster average size $S(p)$ in the low-density domain $(p<pc)$

The method consists in examining the average size $S(p)$ of finite-size clusters and looking for the concentration threshold above which it diverges.

Defining the size of a cluster by the number of atoms it is made up of, the average size is given by

$$S(p)=\sum_{s=0}^{s_{max}} s^2 n(s) \Big/ \sum_{s=0}^{s_{max}} s n(s)\ . \tag{10a}$$

More generally, defining the $k$th moment of $n(s)$ by

$$M_k=\sum_{s=0}^{s_{max}} s^k n(s)\ , \tag{10b}$$

it is seen that the average size $S(p)$ is nothing but the reduced second-order moment $m_2$:

$$S(p)=m_2=M_2/M_1\ .$$

In the low-density domain, $M_1$ is identically equal to the concentration $p$. Developing the perimeter polynomials with respect to $p$ (by using the identity $q=1-p$), and dividing it by $p$, yields the average size $S(p)$, which can be written as

$$S(p)=\sum_{i=0}^{s_{max}-1} a_i p^i\ .$$

The higher-order term corresponds now to $s_{max}-1$, i.e., 15 (because of dividing by $M_1=p$). The 16 coefficients are gathered in the third column of Table III.

From scaling arguments, it is known that $S(p)$ diverges at $p_c$ with a critical exponent $\gamma$, according to

$$S(p)=A_2(p_c-p)^{-\gamma} \quad \text{for } p\rightarrow p_c^-\ , \tag{11}$$

where $A_2$ is the amplitude of the divergence and $\gamma$ is supposed to depend only on the space dimensionality and not on the connectivity of the particular lattice.

The ratio method can be first tried to get a first evalua-

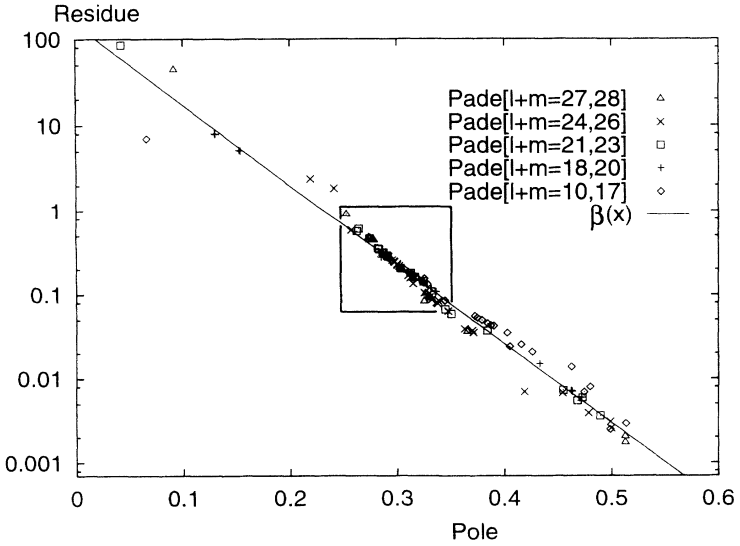


FIG. 6. The (pole, residue) pairs for the Padé approximants to $P'(q)/P(q)$: illustration of the exponential relationship. Only the poles belonging to the boxed area $(0.25<p<0.35)$ will be used to determine the fitting expression of $\beta(p)$.

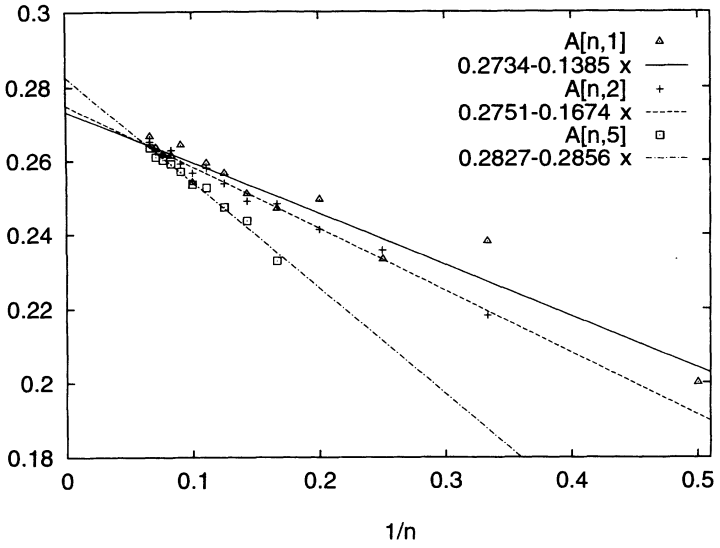


FIG. 7. Plot of $A[n,j]=(a_{n-j}/a_n)^{1/j}$ vs $1/n$ for the series $S(p)$ and of the best linear fit for $j=1,2,5$.

tion of the radius of convergence. Plotting $A[n,1]=a_{n-1}/a_n$ as a function of $1/n$ shows an irregularly oscillatory behavior (Fig. 7), which can be roughly least squared by a straight line giving $p_c=0.2734$. The oscillations can be damped by plotting instead $A[n,j]=(a_{n-j}/a_n)^{(1/j)}$, with $j$ larger than unity; the agreement with a straight line is improved, but the resulting value for $p_c$ raises continuously from 0.2751 ($j=2$) to 0.2827 ($j=5$), which is highly unpleasant. Converting the divergence of $S(p)$ to a simple pole by raising the initial series to the power $1/\gamma$ (with a trial value $\gamma=1.80$), we obtain a new series $(u_n p^n)$. Applying the ratio method to $(u_n)$ and plotting $U[n,j]=(u_{n-j}/u_n)^{(1/j)}$ shows that the variation with $1/n$ is nearly suppressed as expected, but the remaining scattering is still too important to deduce an accurate result (Fig. 8). We tried also more refined evaluation,[36] but the result is still worse than with the classical ratio method.

The analysis by $D$ log Padé approximants $(l,m)$ of $S(p)$ is performed in the same way as for $P(q)$. All the pairs $(\gamma,p_c)$ have been plotted in Fig. 9 in the range $0.25<p_c<0.35$, which contains almost all the available points. Although it is less spectacular than for $\beta$, it is remarkable to note that, here too, a simple exponential fit can represent the results over more than one order of magnitude. It can be checked that adding one more term in $S(p)$ produces more and more approximants with a pole in the expected region, with a (generally) decreasing scattering around the average curve. In the present case, however, unlike the case of $P(q)$, the lower-order approximants ($5\le l+m\le 10$), which are of lower quality by construction, give results which depart systematically and significantly from the values obtained through the approximants ($11\le l+m\le 14$). This is the reason why we excluded them from the fit performed in the restricted range (0.274,0.279) represented by the boxed area. The resulting expression is

$$\gamma(p)=1.059\times 10^{-4}\exp(34.993p)\ . \tag{12}$$

Although this fitting procedure can seem somewhat

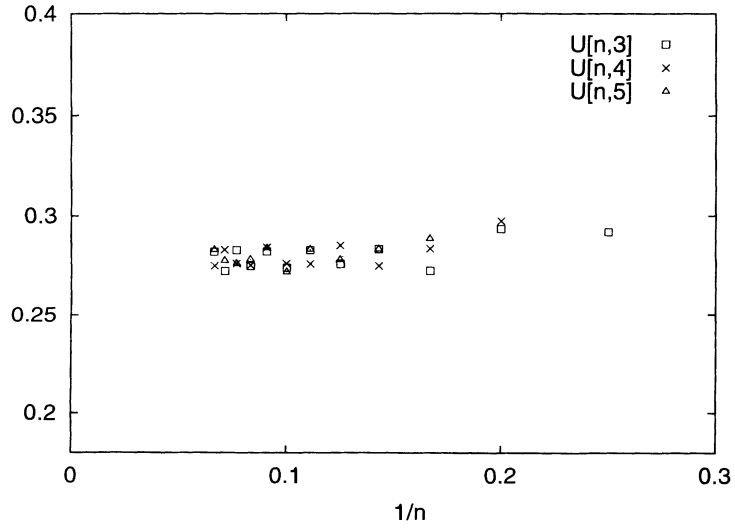


FIG. 8. Plot of $U[n,i]=(u_{n-i}/u_n)^{1/i}$, with $i=3,4,5$ for the series $S(p)^{1/1.80}$.

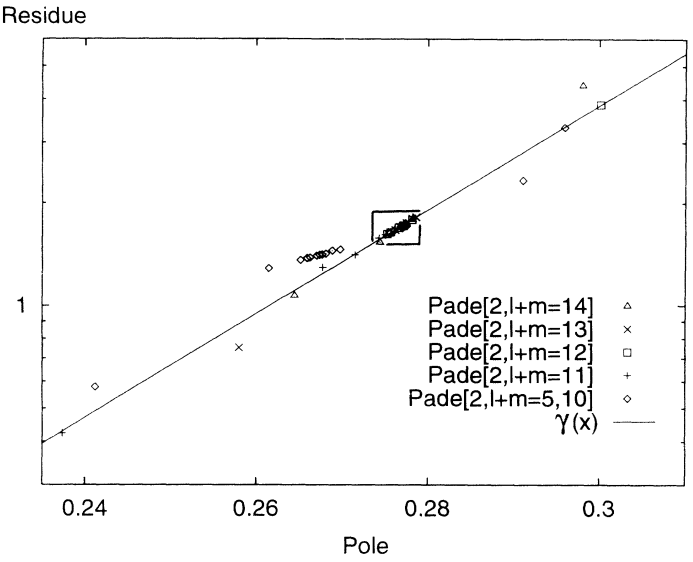


FIG. 9. The (pole, residue) pairs for the Padé approximants to $S'(p)/S(p)$: illustration of the exponential relationship. The poles of the lower-order approximants denoted by diamonds depart significantly from the others. Only the poles belonging to the boxed area ($0.274 < p < 0.279$) will be used to determine the fitting expression of $\gamma(p)$.

artificial for $\gamma$ for such a small interval where the fit is very close to a simple linear one, we kept it in for consistence with the interpolation procedure for $\beta$.

Here, again, it can be checked that diagonal approximants are not systematically the best ones, at the benefit of more exotic off-diagonal approximants.

We tried also a standard Padé analysis applied to the series $(u_n)=(a_n)^{(1/\gamma)}$ with the approximants $l+m=10-15$ and $|l-m|\leq 5$. The values of the poles are found in a narrower range with average values of $0.2784\pm 0.004$. A careful inspection of a sequence of diagonal (or near-diagonal) approximants shows a noticeable drift on the average value of $p_c$, which did not yet reach its asymptotic limit with the higher-order approximants ($l+m=15$) presently available (last column of Table IV). This conclusion is not qualitatively altered if another reasonable value of $\gamma$ is tried: When $\gamma$ is enhanced (or decreased) by 0.015, $p_c$ is increased (or decreased) by 0.0002 only. We conclude that a part of the difficulty to converge toward a stable value is clearly due to the insufficient number of available terms in the series, but that the final value of $p_c$ should be anyway smaller than 0.278 18.

Another cause of this difficulty to converge rapidly might be the presence of a confluent singularity, which is usually represented by a correction term to formula (11) with another (noninteger) exponent $\Delta$:

$$S(p)=A_2(p_c-p)^{-\gamma}[1+A_{21}(p_c-p)^{\Delta}+\cdots], \quad (13)$$

where a value significantly different from unity is expected for $\Delta$. We give in Appendix C the account of two attempts to determine the possible presence of such a corrective term. The results are not contradictory with a recent work which shows that a confluent singularity in 3D percolation is probably not present.[37]

At last, in the spirit of previous work,[38] several mappings of the variable $p/p_c$ onto a new variable $y$ by a Euler transformation have been tried in order to move other singularities as far away from the origin as possible and let the singularity at $y=1$ be the closest. But the results are not better than without any mapping.

TABLE IV. Estimates for $p_c$ through the $(l,m)$ Padé approximants to $S(p)^{1/\gamma}$ with $\gamma=1.80$. The first column gives $l+>m$. The next nine columns give the estimate with $|l-m|\leq 4$ and $l,m\geq 4$. The estimate is considered as unreliable if a nearby pole with positive real part lies within 0.25 of $p_c$ (NP) or if the pole is not the closest to the origin (NC). The last column takes the average over reliable values only. The symbol $[(l+m)/2]$ denotes the integer part of $(l+m)/2$.

| | | | | | $n=[(l+m)/2]$ | | | | | |
|---|---|---|---|---|---|---|---|---|---|---|
| $l+m$ | $n-2,n+3$ | $n-2,n+2$ | $n-1,n+2$ | $n-1,n+1$ | $n,n+1$ | $n,n$ | $n+1,n$ | $n+1,n-1$ | $n+2,n-1$ | $n+2,n-2$ | $n+3,n-2$ | Average |
| 6 | | | | | | 0.282 63 | | | | | | 0.282 63 |
| 7 | | | | | | | | | | | | |
| 8 | | | | | | 0.276 84 | | | | | | 0.276 840 |
| 9 | | | | | 0.283 12 | | 0.279 53 | | | | | 0.281 325 |
| 10 | | | | 0.279 73 | | 0.279 02 | | 0.279 12 | | | | 0.279 290 |
| 11 | | | 0.281 05 NC | | 0.278 83 | | 0.278 73 | | 0.278 89 | | | 0.278 816 |
| 12 | | 0.277 87 | | 0.276 74 NP | | 0.279 11 NC | | 0.279 29 NC | | 0.278 39 | | 0.278 130 |
| 13 | 0.278 57 | | 0.279 12 | | 0.278 22 | | 0.275 07 NP | | 0.278 25 | | 0.278 28 | 0.278 467 |
| 14 | | 0.278 47 | | 0.278 25 | | 0.278 24 | | 0.278 36 | | 0.278 32 | | 0.278 328 |
| 15 | 0.278 63 NC | | 0.278 03 | | 0.278 22 | | 0.278 09 | | 0.278 28 | | 0.278 29 | 0.278 182 |

To close this section, in view of the presently available terms of the series, it cannot be concluded that a correction term is necessary to describe the divergence of $S(p)$.

### C. Examining the higher-order moments of $n(s)$ in the low-density domain ($p < p_c$)

A similar $D$ log Padé analysis can be performed on the higher-order moments of $n(s)$, thanks to a recent conjecture[37] which states that the $k$th-order moment diverges at $p_c$ like

$$M_k = A_k(p_c - p)^{-\gamma_k} \quad \text{for } p \to p_c - \tag{14}$$

with $\gamma_k = (k-1)\gamma + (k-2)\beta$. Although this result stands for the bond percolation problem, we made the reasonable assumption that it should hold, too, for the site problem. The $D$ log Padé approximants are evaluated for moments up to sixth order, beyond which too few poles are found in the range (0.25,0.30). The residues are plotted as a function of the poles as before, and it turns out that the same type of exponential fit can be performed for any of these moments. We have gathered in Appendix D the (pole, residue) plots for each moment of $k$th order together with the expressions of the fitting functions $\gamma_k(p)$.

### D. Most probable triplet ($p_c, \beta, \gamma$) consistent with the whole body of our results

At this stage, all the previous work performed up to now is entirely contained in the expressions $\beta(p)$ and $\gamma_k(p)$ with the convention that $\gamma_2(p)$ is the function $\gamma(p)$ which has been determined in Sec. III B. These results can be used in three different ways.

(i) Considering the most recent values of $\beta$ and $\gamma$ (denoted by $\beta_0$ and $\gamma_0$, respectively) as the best ones, we determine the percolation threshold for our lattice by minimizing the sum of the squared deviations from our results:

$$\sigma = (\beta_0 - \beta(p))^2 + \sum_{i=2}^{6} [(i-1)\gamma_0 + (i-2)\beta_0 - \gamma_i(p)]^2/(2i-3)^2 . \tag{15}$$

The denominator $(2i-3)^2$ is introduced to give the same weight to any of the determinations of the critical exponents or any of the linear combinations which appear in the $\gamma_k$'s.

Several possible couples of $(\beta_0, \gamma_0)$ have been tried: either from Ref. 37 or from the best computer estimate obtained up to now,[39] which lies in the confidence interval quoted by Ref. 37.

The value of $p_c$ which minimizes the above sum depends on the values of $\beta_0$ and $\gamma_0$. In the four cases corresponding to the ends of the confidence intervals for $\beta$ and $\gamma$ ($\beta_0 = 0.405 \pm 0.025$), ($\gamma_0 = 1.805 \pm 0.020$), the resulting value for $p_c$ remains constrained in the narrow range

$$0.2775 < p_c < 0.2785 .$$

(ii) A second choice consists in giving an infinite weight to the "direct" determination of $\beta$ and $\gamma$ by requiring that the final values of $\beta$ and $\gamma$ lie on the curve $\beta(p)$ and $\gamma(p)$. The argument for this could be that the corresponding curves are fitted on many more data than the curves corresponding to the $\gamma_k$'s with $k > 2$. In the above summation, it corresponds to the case where the first two terms are set identically to zero [$\beta_0 = \beta(p)$, $\gamma_0 = \gamma(p)$]. As a consequence, the determination of $p_c$ rests only on the $\gamma_k$'s (with $k > 2$), that is, only on the quality of the conjecture about the behavior of all the moments of $n(s)$. The result of the minimization yields

$$p_c = 0.2779, \quad \beta = \beta(p_c) = 0.403, \quad \gamma = \gamma(p_c) = 1.771 .$$

(iii) At last, a more severe test consists in looking for the triplet $(\beta_0, \gamma_0, p_c)$ which minimizes the sum. Equating to zero the three partial derivatives of $\sigma$ with respect to $\beta_0$, $\gamma_0$, and $p_c$ yields three equations. The first two are linear in $\beta_0$ and $\gamma_0$ and can be easily solved to get $\beta_0$ and $\gamma_0$ as functions of $p_c$. The third equation depends then only on $p_c$ and is easily solved by trial and error:

$$p_c = 0.2776, \quad \beta = 0.414, \quad \gamma = 1.763 .$$

The most remarkable result is that the final value obtained for $p_c$ is rather insensitive to the minimization procedure.

As a result, it can be proposed that the threshold should reasonably belong to the interval

$$0.2775 < p_c < 0.2782 ,$$

where the upper limit has been chosen according to the result of the Padé analysis performed on the series raised to the power $1/\gamma$ in Sec. III B.

Whereas the classical analysis by $D$ log Padé approximants to the percolation probability and to the average cluster size yields only the relationships $\beta(p_c)$ and $\gamma(p_c)$, respectively, it is concluded from this section that the information contained in the higher-order moments of the cluster density function can be used to improve the determination of the threshold and to propose a rather tight range for the expected final value. The corresponding values of $\beta$ and $\gamma$ are in reasonable agreement with the best estimates available at the present time.

## IV. COMPARISON WITH THE MEAN-FIELD RESULT AND CONCLUSIONS

The mean-field formulation of the diffusion problem consists in describing in detail the movement of the dumbbell defect in a small region of the alloy defined by the occupancy of the sites and embedding this region in an average medium characterized by a uniform effective frequency $X$. In the present case, the small region in question is that depicted in Fig. 2 minus the six most outward vertices of the cluster and it contains 30 lattice sites. The contribution of each region to the total diffusivity requires the calculation of correlation effects and can be expressed as a function of $W_R$, $W_L$, and $X$. These contributions are then weighted by the occurrence probability of the configuration in the alloy and summed altogether to yield the diffusion coefficients $D_{A^*}$ and $D_{B^*}$ of $A^*$ and $B^*$ tracers. The effective frequency $X$ is at last determined by solving a self-consistency equation

$$C_A D_{A*} + C_B D_{B*} = D_{X*} ,$$

in which $D_{X*}$ stands for the self-diffusion coefficient of the average medium and is a function of $X$ only. The most remarkable feature of this very simple procedure lies in the fact that, in the limit where $W_R / W_L$ tends to infinity, the percolation threshold appears naturally as that critical concentration below which the solution of the self-consistency equation is identically zero. This corresponds to the physical situation where the defect is trapped in clusters entirely surrounded by immobile atoms and where long-range diffusivity is forbidden. It is remarkable that the value of 0.280 found for the threshold by this mean-field approximation is very close to the exact one given by the series method.[26]

The general conclusions concerning the diffusion problem can be summarized as follows.

(i) The models for electrical conductivity cannot be used straightforwardly for describing the mass transport in alloys. The existence of point defects and of the corresponding jump mechanism may induce new types of percolation.

(ii) The percolative regime of mass transport by a given atomic mechanism can be reduced to a site percolation problem whenever the walk of the defect does not alter the shape of the clusters which are present in the alloy: This requirement is met by the vacancy mechanism studied in the past[41] as well as by the dumbbell interstitial mechanism of the present study for some of its variants.

(iii) Whenever condition (ii) is not fulfilled, the diffusion problem pertains to other, and yet undefined, types of percolation.

## ACKNOWLEDGMENT

We thank J. Zinn-Justin for his valuable and fruitful comments about the choice of Padé approximants.

## APPENDIX A: PERIMETER POLYNOMIALS FOR CLUSTERS CONTAINING UP TO 14 ATOMS

### 1. Origin along $Ox$

$$D_{1x} = q^8, \quad D_{2x} = 4q^{12}, \quad D_{3x} = 10q^{15} + 12q^{16}, \quad D_{4x} = 2q^{16} + 35q^{18} + 65q^{19} + 38q^{20} ,$$

$$D_{5x} = 24q^{19} + 7q^{20} + 118q^{21} + 395q^{22} + 317q^{23} + 110q^{24} ,$$

$$D_{6x} = 19q^{21} + 161q^{22} + 114q^{23} + 651q^{24} + 2048q^{25} + 2398q^{26} + 1388q^{27} + 322q^{28} ,$$

$$D_{7x} = 12q^{22} + 14q^{23} + 242q^{24} + 1127q^{25} + 1345q^{26} + 3948q^{27} + 11\,331q^{28} + 16\,368q^{29} + 12\,931q^{30} + 5625q^{31} + 926q^{32} ,$$

$$D_{8x} = 38q^{24} + 239q^{25} + 343q^{26} + 2098q^{27} + 8197q^{28} + 12\,793q^{29} + 26\,443q^{30} + 67\,903q^{31} + 107\,998q^{32} + 106\,698q^{33} + 63\,500q^{34} + 21\,270q^{35} + 2642q^{36} ,$$

$$D_{9x} = 6q^{24} + 37q^{25} + 90q^{26} + 660q^{27} + 2471q^{28} + 5062q^{29} + 18\,286q^{30} + 60\,110q^{31} + 109\,491q^{32} + 196\,969q^{33} + 430\,659q^{34} + 725\,650q^{35} + 814\,576q^{36} + 611\,163q^{37} + 289\,538q^{38} + 76\,922q^{39} + 7552q^{40} ,$$

$$D_{10x} = 20q^{25} + 35q^{26} + 94q^{27} + 578q^{28} + 2046q^{29} + 7704q^{30} + 24\,834q^{31} + 57\,650q^{32} + 161\,565q^{33} + 457\,494q^{34} + 888\,440q^{35} + 1\,531\,879q^{36} + 2\,940\,700q^{37} + 4\,938\,182q^{38} + 6\,088\,926q^{39} + 5\,318\,749q^{40} + 3\,209\,626q^{41} + 1\,245\,499q^{42} + 270\,288q^{43} + 21\,686q^{44} ,$$

$$D_{11x} = 11q^{25} + 314q^{28} + 756q^{29} + 1694q^{30} + 8073q^{31} + 28\,149q^{32} + 85\,639q^{33} + 248\,214q^{34} + 582\,851q^{35} + 1\,430\,522q^{36} + 3\,589\,352q^{37} + 7\,102\,336q^{38} + 12\,120\,814q^{39} + 21\,209\,772q^{40} + 34\,618\,820q^{41} + 45\,074\,467q^{42} + 44\,036\,715q^{43} + 31\,464\,361q^{44} + 15\,769\,546q^{45} + 5\,133\,090q^{46} + 930\,037q^{47} + 61\,696q^{48} ,$$

$$D_{12x} = q^{24} + 200q^{28} + 358q^{30} + 3972q^{31} + 12\,026q^{32} + 28\,548q^{33} + 105\,765q^{34} + 331\,988q^{35} + 913\,405q^{36} + 2\,396\,987q^{37} + 5\,597\,621q^{38} + 12\,698\,587q^{39} + 28\,899\,682q^{40} + 56\,686\,630q^{41} + 96\,543\,472q^{42} + 159\,303\,933q^{43} + 250\,529\,979q^{44} + 334\,909\,921q^{45} + 354\,395\,896q^{46} + 287\,087\,247q^{47} + 172\,795\,737q^{48} + 73\,614\,817q^{49} + 20\,442\,704q^{50} + 3\,133\,608q^{51} + 175\,654q^{52} ,$$

$$D_{13x}=18q^{27}+191q^{30}+2305q^{31}+1824q^{32}+9317q^{33}+54\,540q^{34}+166\,918q^{35}$$
$$+399\,026q^{36}+1\,252\,729q^{37}+3\,649\,121q^{38}+9\,383\,659q^{39}+22\,983\,847q^{40}+52\,206\,242q^{41}$$
$$+112\,421\,516q^{42}+237\,538\,661q^{43}+455\,089\,387q^{44}+771\,991\,950q^{45}+1\,230\,481\,444q^{46}$$
$$+1\,867\,387\,844q^{47}+2\,517\,209\,392q^{48}+2\,812\,445\,658q^{49}+2\,505\,348\,940q^{50}+1\,730\,156\,439q^{51}$$
$$+895\,463\,628q^{52}+329\,568\,615q^{53}+79\,036\,271q^{54}+10\,392\,784q^{55}+498\,284q^{56}\ ,$$

$$D_{14x}=17q^{29}+178q^{30}+261q^{31}+231q^{32}+5316q^{33}+29\,008q^{34}+51\,790q^{35}+160\,050q^{36}$$
$$+699\,251q^{37}+2\,056\,008q^{38}+5\,064\,144q^{39}+14\,244\,608q^{40}+38\,546\,909q^{41}+94\,097\,686q^{42}$$
$$+218\,693\,214q^{43}+479\,170\,173q^{44}+991\,355\,191q^{45}+1\,981\,818\,090q^{46}+3\,687\,848\,704q^{47}$$
$$+6\,202\,751\,007q^{48}+9\,678\,831\,556q^{49}+14\,280\,798\,796q^{50}+19\,201\,134\,455q^{51}+22\,231\,810\,067q^{52}$$
$$+21\,264\,177\,396q^{53}+16\,332\,030\,595q^{54}+9\,796\,281\,331q^{55}+4\,424\,842\,014q^{56}+1\,424\,138\,394q^{57}$$
$$+298\,031\,522q^{58}+33\,997\,583q^{59}+1\,412\,244q^{60}\ .$$

### 2. Origin along *Oy*

$$D_{1y}=q^{8},\quad D_{2y}=4q^{12},\quad D_{3y}=10q^{15}+12q^{16},\quad D_{4y}=q^{16}+34q^{18}+67q^{19}+38q^{20}\ ,$$

$$D_{5y}=16q^{19}+5q^{20}+123q^{21}+383q^{22}+335q^{23}+110q^{24}\ ,$$

$$D_{6y}=11q^{21}+129q^{22}+92q^{23}+625q^{24}+2058q^{25}+2428q^{26}+1452q^{27}+322q^{28}\ ,$$

$$D_{7y}=6q^{22}+6q^{23}+182q^{24}+939q^{25}+1151q^{26}+3850q^{27}+11\,275q^{28}+16\,606q^{29}$$
$$+13\,235q^{30}+5875q^{31}+910q^{32}\ ,$$

$$D_{8y}=15q^{24}+147q^{25}+215q^{26}+1770q^{27}+7115q^{28}+11\,317q^{29}+25\,793q^{30}+67\,591q^{31}$$
$$+108\,680q^{32}+108\,870q^{33}+65\,573q^{34}+21\,990q^{35}+2586q^{36}\ ,$$

$$D_{9y}=2q^{24}+11q^{25}+392q^{27}+1827q^{28}+3648q^{29}+15\,877q^{30}+54\,120q^{31}$$
$$+99\,765q^{32}+190\,290q^{33}+428\,947q^{34}+727\,104q^{35}+827\,564q^{36}+626\,989q^{37}+299\,418q^{38}$$
$$+78\,782q^{39}+7416q^{40}\ ,$$

$$D_{10y}=4q^{25}+7q^{26}+46q^{27}+280q^{28}+1016q^{29}+5572q^{30}+19\,620q^{31}+45\,672q^{32}$$
$$+142\,162q^{33}+420\,930q^{34}+827\,058q^{35}+1\,476\,399q^{36}+2\,916\,412q^{37}+4\,948\,510q^{38}$$
$$+6\,154\,872q^{39}+5\,433\,623q^{40}+3\,301\,696q^{41}+1\,285\,625q^{42}+275\,304q^{43}+21\,322q^{44}\ ,$$

$$D_{11y}=q^{25}+106q^{28}+244q^{29}+1022q^{30}+4947q^{31}+17\,629q^{32}+65\,981q^{33}+205\,182q^{34}$$
$$+488\,719q^{35}+1\,277\,442q^{36}+3\,346\,148q^{37}+6\,705\,522q^{38}+11\,696\,118q^{39}+20\,973\,186q^{40}$$
$$+34\,636\,794q^{41}+45\,461\,751q^{42}+44\,777\,313q^{43}+32\,247\,817q^{44}+16\,234\,698q^{45}+5\,286\,066q^{46}$$
$$+943\,759q^{47}+60\,636q^{48}\ ,$$

$$D_{12y}=40q^{28}+161q^{30}+1788q^{31}+5500q^{32}+19\,028q^{33}+73\,073q^{34}+235\,443q^{35}$$
$$+731\,858q^{36}+2\,058\,731q^{37}+4\,871\,653q^{38}+11\,489\,567q^{39}+27\,155\,722q^{40}+54\,063\,814q^{41}$$
$$+93\,430\,992q^{42}+157\,157\,391q^{43}+250\,289\,936q^{44}+337\,112\,847q^{45}+359\,265\,481q^{46}$$
$$+293\,033\,667q^{47}+177\,396\,503q^{48}+75\,787\,859q^{49}+21\,001\,754q^{50}+3\,169\,780q^{51}+172\,374q^{52}\ ,$$

$$D_{13y}=2q^{27}+49q^{30}+743q^{31}+680q^{32}+5120q^{33}+28\,865q^{34}+94\,746q^{35}+283\,870q^{36}$$
$$+943\,903q^{37}+2\,807\,530q^{38}+7\,789\,241q^{39}+20\,186\,429q^{40}+46\,631\,648q^{41}+103\,046\,906q^{42}$$
$$+224\,437\,939q^{43}+436\,870\,461q^{44}+749\,731\,277q^{45}+1\,212\,426\,717q^{46}+1\,862\,409\,562q^{47}$$
$$+2\,529\,758\,918q^{48}+2\,844\,177\,082q^{49}+2\,549\,168\,328q^{50}+1\,770\,317\,069q^{51}+920\,142\,698q^{52}$$
$$+339\,134\,894q^{53}+80\,999\,311q^{54}+10\,480\,540q^{55}+488\,412q^{56}\ ,$$

$$D_{14y}=3q^{29}+40q^{30}+67q^{31}+81q^{32}+204q^{33}+12\,114q^{34}+24\,062q^{35}+96\,544q^{36}$$
$$+430\,548q^{37}+1\,358\,224q^{38}+3\,799\,832q^{39}+11\,310\,898q^{40}+31\,346\,275q^{41}+80\,442\,753q^{42}$$
$$+195\,098\,206q^{43}+435\,775\,385q^{44}+919\,395\,582q^{45}+1\,881\,480\,438q^{46}+3\,555\,351\,740q^{47}$$
$$+6\,042\,187\,233q^{48}+9\,535\,146\,122q^{49}+14\,220\,256\,662q^{50}+19\,268\,055\,753q^{51}+22\,439\,669\,438q^{52}$$
$$+21\,580\,542\,198q^{53}+16\,661\,936\,725q^{54}+10\,039\,811\,013q^{55}+4\,548\,662\,064q^{56}+1\,464\,132\,020q^{57}$$
$$+304\,684\,546q^{58}+34\,186\,309q^{59}+1\,383\,972q^{60}\ .$$

### 3. Origin along *Oz*

$$D_{1z}=q^{8},\quad D_{2z}=4q^{12},\quad D_{3z}=12q^{15}+12q^{16},\quad D_{4z}=42q^{18}+84q^{19}+32q^{20}\ ,$$

$$D_{5z}=8q^{19}+6q^{20}+173q^{21}+440q^{22}+404q^{23}+80q^{24}\ ,$$

$$D_{6z}=6q^{21}+106q^{22}+82q^{23}+749q^{24}+2530q^{25}+2974q^{26}+1544q^{27}+208q^{28}\ ,$$

$$D_{7z}=4q^{23}+152q^{24}+826q^{25}+1038q^{26}+4346q^{27}+13\,964q^{28}+20\,930q^{29}+15\,378q^{30}$$
$$+5492q^{31}+576q^{32}\ ,$$

$$D_{8z}=q^{24}+58q^{25}+150q^{26}+1676q^{27}+6708q^{28}+11\,020q^{29}+28\,194q^{30}+83\,362q^{31}$$
$$+138\,660q^{32}+131\,220q^{33}+70\,703q^{34}+19\,140q^{35}+1600q^{36}\ ,$$

$$D_{9z}=216q^{27}+1300q^{28}+2822q^{29}+15\,412q^{30}+54\,922q^{31}+101\,808q^{32}+207\,115q^{33}$$
$$+525\,284q^{34}+923\,198q^{35}+1\,025\,322q^{36}+717\,530q^{37}+304\,066q^{38}+65\,360q^{39}+4364q^{40}\ ,$$

$$D_{10z}=28q^{27}+144q^{28}+622q^{29}+4340q^{30}+16\,002q^{31}+39\,508q^{32}+141\,713q^{33}$$
$$+442\,662q^{34}+882\,274q^{35}+1\,631\,684q^{36}+3\,518\,224q^{37}+6\,264\,114q^{38}+7\,694\,994q^{39}$$
$$+6\,463\,956q^{40}+3\,612\,826q^{41}+1\,245\,708q^{42}+217\,872q^{43}+11\,724q^{44}\ ,$$

$$D_{11z}=84q^{28}+200q^{29}+620q^{30}+3240q^{31}+14\,750q^{32}+56\,688q^{33}+180\,750q^{34}$$
$$+458\,166q^{35}+1\,311\,181q^{36}+3\,611\,876q^{37}+7\,374\,422q^{38}+13\,158\,452q^{39}+25\,120\,308q^{40}$$
$$+43\,456\,510q^{41}+57\,098\,660q^{42}+54\,390\,984q^{43}+36\,977\,662q^{44}+17\,095\,736q^{45}+4\,904\,676q^{46}$$
$$+708\,964q^{47}+31\,668q^{48}\ ,$$

$$D_{12z}=48q^{28}+72q^{30}+1704q^{31}+4869q^{32}+12\,360q^{33}+56\,758q^{34}+214\,624q^{35}$$
$$+677\,082q^{36}+1\,950\,872q^{37}+4\,819\,512q^{38}+12\,093\,152q^{39}+29\,888\,494q^{40}+60\,766\,156q^{41}$$
$$+106\,947\,334q^{42}+187\,746\,522q^{43}+311\,277\,967q^{44}+423\,202\,892q^{45}+441\,862\,516q^{46}$$
$$+345\,877\,722q^{47}+196\,897\,096q^{48}+76\,936\,008q^{49}+18\,667\,958q^{50}+2\,268\,124q^{51}+86\,408q^{52}\ ,$$

$$D_{13z}=4q^{27}+48q^{30}+984q^{31}+160q^{32}+3329q^{33}+26\,200q^{34}+84\,452q^{35}+223\,362q^{36}$$
$$+827\,404q^{37}+2\,693\,721q^{38}+7\,629\,168q^{39}+20\,068\,260q^{40}+48\,014\,894q^{41}+110\,954\,384q^{42}$$
$$+250\,827\,432q^{43}+499\,035\,878q^{44}+870\,526\,681q^{45}+1\,449\,488\,639q^{46}+2\,300\,112\,498q^{47}$$
$$+3\,165\,679\,140q^{48}+3\,521\,810\,180q^{49}+3\,065\,290\,376q^{50}+2\,033\,748\,184q^{51}+989\,803\,888q^{52}$$
$$+332\,196\,493q^{53}+69\,082\,680q^{54}+7\,179\,604q^{55}+237\,916q^{56}\ ,$$

$$D_{14z}=4q^{29}+82q^{30}+8q^{31}+48q^{32}+1932q^{33}+12\,866q^{34}+15\,012q^{35}+76\,751q^{36}+404\,563q^{37}$$
$$+1\,283\,612q^{38}+3\,359\,068q^{39}+10\,571\,496q^{40}+31\,245\,429q^{41}+81\,862\,214q^{42}+201\,173\,138q^{43}$$
$$+462\,580\,807q^{44}+1\,009\,983\,737q^{45}+2\,129\,956\,080q^{46}+4\,109\,529\,312q^{47}+7\,093\,525\,026q^{48}$$
$$+11\,432\,339\,712q^{49}+17\,475\,978\,914q^{50}+24\,017\,440\,696q^{51}+27\,863\,727\,773q^{52}+26\,263\,150\,230q^{53}$$
$$+19\,591\,556\,440q^{54}+11\,231\,465\,215q^{55}+4\,745\,789\,274q^{56}+1\,385\,506\,438q^{57}+250\,016\,088q^{58}$$
$$+22\,555\,140q^{59}+652\,836q^{60}\ .$$

### 4. Comments

The minimum perimeter for an $s$-atom cluster is given by the smallest power in the $q$ expansion; this minimum is *not* a strictly monotonously increasing function of $s$, since we can point out several pairs of consecutive polynomials having the same lowest order (for instance, $D_{8x}$ and $D_{9x}$, $D_{10x}$ and $D_{11x}$, . . . ). It is not even a monotonous function in the wide sense, as can be seen by comparing $D_{11x}$ and $D_{12x}$, where the smaller perimeter is obtained for the bigger cluster. This is a consequence of the existence of forbidden sites: Figure 5 shows the most compact configuration of an 11-atom cluser; this cluster is the incomplete shell around a forbidden site. The addition of the 12th atom closes the shell by occupying one site of the previous perimeter without adding any new perimeter site, since the neighbors of the newly occupied site which do not belong the cluster ($V_5, V_8, V_9, V_{11}$) were already countered as neighbors of atoms already present in the cluster ($V_5$ is already a first neighbor of 5, etc.). This explains the decrease by 1 of the smallest order appearing in the polynomials $D_{11x}$ and $D_{12x}$. This is very worrying since the higher-order term available in the power expansion of the percolation probability $P(q)$ stems from the smallest perimeter of the largest cluster of size $s_{\max}$ counted up to now. If clusters of size $s_{\max}+1$ are added, their counting might change the last term(s) of $P(q)$. However, it is reasonable to assume that this irregular behavior will be observed only when a shell around a forbidden site will close up, which happens for $11\rightarrow 12$, $19\rightarrow 20$ (two neighbor shells sharing four common sites, etc.). The present calculation with 16 sites should not be altered by this drawback, and the presently available coefficients in the series expansion of $P(q)$ should not be modified if the counting of larger clusters is undertaken.

## APPENDIX B: COMPARISON OF THE REDNER'S AND MERTENS ENUMERATION ALGORITHMS

This appendix compares the algorithm for enumerating clusters due to Redner,[32] which has been used in our study, with a more recent one due to Mertens.[34]

Both of them generate all clusters up to a given size $s_{\max}$ in a recursive way: Given an $s$ cluster, they build all possible $(s+1)$ clusters by adding a new cluster site. The choice of this new site is constrained by the requirement of generating each cluster exactly once in the recursive tree. Redner's algorithm keeps a list of the forbidden sites, which implies that each new candidate must be compared to the list in order to be rejected or accepted: This selection mechanism is apparently more time consuming than Mertens' algorithm, which keeps a list of the allowed sites only. For sake of space, we refer the reader to the original papers for the details of each algorithm and their Fortran translation and describe hereafter only those modifications we have done to adapt the general scheme to our particular lattice.

### 1. Mertens' method

For the lattice under consideration, the adjacency vectors are not constant, but vary from site to site: They must be calculated once for all at the beginning and stored in a matrix NVOIS(NN,NLATT). Further, since two sites belonging to the cluster can share the same blocked site as a first neighbor, the newly blocked sites which are added to the set of "count" sites by the last new site added to the cluster must be traced in a matrix NCOUNT(4,NAMAS) after line 46 of Mertens' algorithm. They must be released and set back to their original "block" state, any time the corresponding site cluster is freed, that is, after a decrease from $s$ to $s-1$ sites (line 78) or after changing the site which is the starting point of the next branch in the generation tree (line 76). The time of computation with Mertens' method amounts to 5, 43, and 352 s for $s_{\max}=9$, 10, and 11, respectively, on a HP-730 workstation.

### 2. Redner's method

We used a modified version of Redner's original one, in which the interrupted loop running over the neighbors (line 4 in Redner's algorithm) is replaced by a loop with fixed limits (1–8 in the present case) together with some rearranging of the subsequent code. We observed a significant reduction of the computational effort by roughly 20% for the larger cluster enumeration. The time of computation with this algorithm amounts then to 3.5, 34, and 273 s for $s_{\max}=9$, 10, and 11, respectively. But, as noted by Mertens, the counting of the perimeter is not closely associated to the generation of the clusters itself; once a cluster is built, its perimeter is calculated (using the perimeter of the previous cluster containing $s-1$ sites as a starting point): The new site replaces one perimeter site of the previous cluster, but adds in neighbors to the new perimeter provided that these neighbors neither belong to the cluster nor to the previously defined perimeter. This restriction mechanism turns out to be very time consuming: For $s_{\max}=10$, the time grows up

to 900 s. The computational speed is therefore reduced by a factor of 30. This is the reason why we calculated the perimeter for clusters up to 14 sites and enumerated their total number (without the perimeter) up to $s_{\max}=16$, which is known to be equivalent to the knowledge of the perimeters up to $s_{\max}=15$.

Noting at last that counting $n+1$ clusters requires roughly 8.6 times more computation for both algorithms, it can be seen that Mertens' method for $n\max=16$ would have required $(8.6)^5$ times 352 s, that is, 4600 h. This time is comparable to the time we spent for our own calculation (3500+1300 h). The conclusion is that we would have obtained one more term in the series $S(p)$ with Mertens' algorithm using the same amount of computational time.

## APPENDIX C: SEARCH FOR CONFLUENT SINGULARITIES

The two following methods have been usefully employed to determine such singularity in 2D percolation problems.[40]

(i) The first method ($M1$) consists in transforming the original series $S(p)$ into a new one according to

$$B(p)=\gamma S(p)-(p_c-p)dS(p)/d_p \ .$$

This new series has a simple pole at $p_c$ with a residue equal to $-\gamma+\Delta$. For a given value of $p_c$ (chosen in the neighborhood of the expected final result), one obtains a graph of $\Delta$ versus the input value $\gamma$ for each Padé approximant to $B(p)$. One then chooses by a trial and error process the triplet $(p_c,\gamma,\Delta)$ where all the approximants converge to the same point.

Actually, not all the Padé aprpoximants are used since the higher-order ones are better of construction. In the present case, we selected approximants with $l+m=13$ and 14 and $|l-m|\leq 5$. We tried several values for $p_c$ in the range $(0.276<p_c<0.279)$. The result is shown for 0.2778 in Fig. 10(a). The overall aspect is not drastically changed in the range (0.2775,0.2785) and thus cannot be used as an indication toward some optimum value for $p_c$. But it deteriorates if $p_c$ is noticeably larger or smaller.

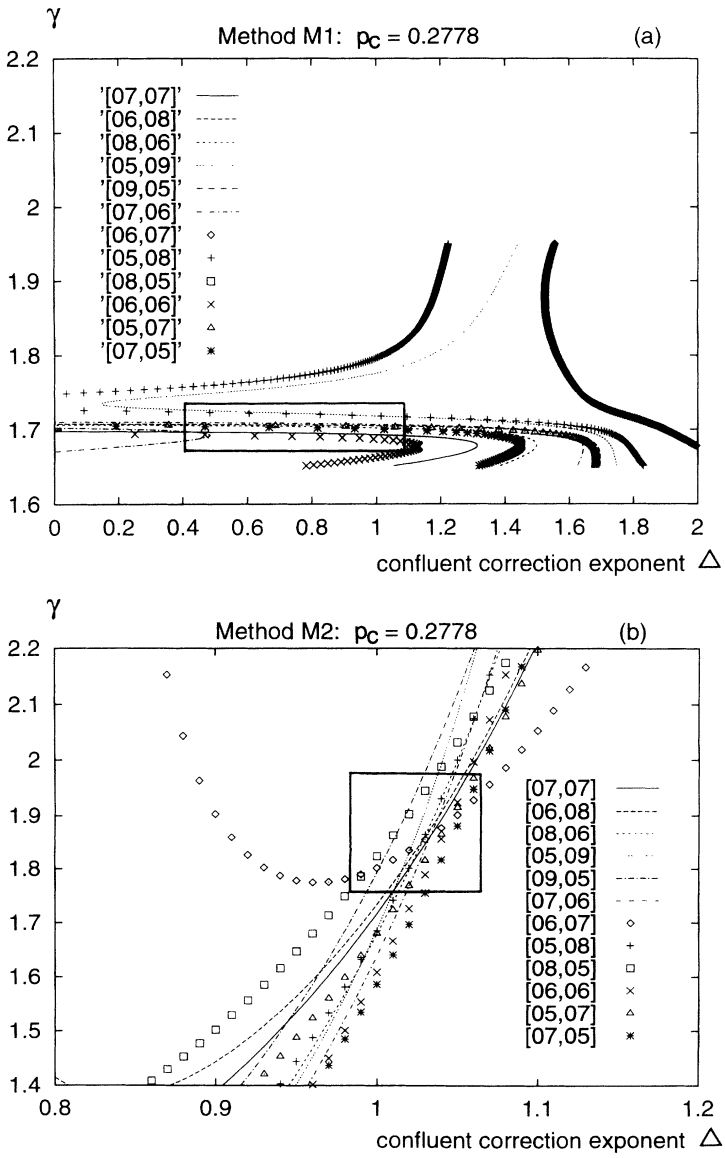


FIG. 10. Graph of $\gamma$ for selected approximants $[l,m]$ to $B(p)$ as a function of the confluent correction exponent $\Delta$ at $p_c=0.277\,80$ for method (a) $M1$ and (b) $M2$. The confluent region is boxed.

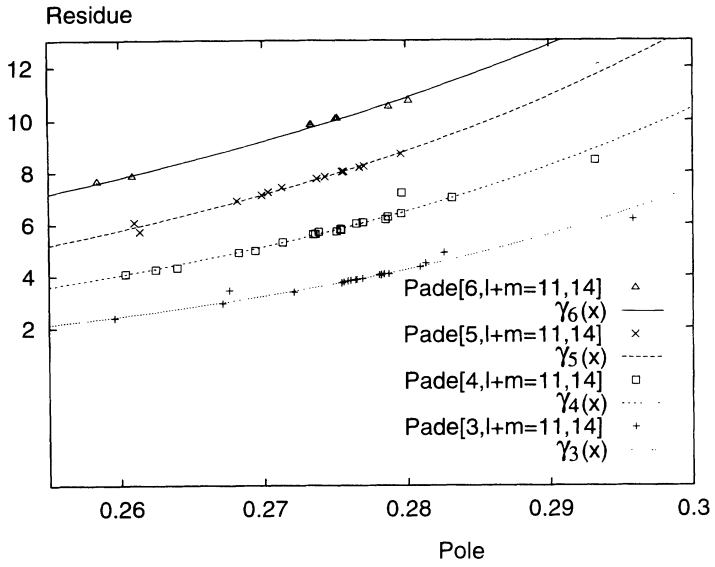


FIG. 11. Plot of the (pole, residue) pairs of the $D$ log Padé approximants to the higher-order moment of the cluster density function $n(s)$. Note the linear scale on the ordinate axis.

The main conclusion is that these approximants are close to one another in the rather large area boxed in the Fig. 10(a):

$$1.68<\gamma<1.73 \quad \text{and} \quad 0.3<\Delta<1.1 \ .$$

The determination of the exponents is not sharp enough to provide us with a clear conclusion about the existence of the corrective term to the scaling law for $S(p)$.

(ii) The second method ($M2$) consists in a mapping of the variable $p/p_c$ onto a new variable $y$ defined by

$$y=1-(1-p/p_c)^{\Delta} \ .$$

Studying the new series $B(y)=S(p(y))$, it is easy to show that its logarithmic derivative has a simple pole at $y=1$ with a residue equal to $-\gamma/\Delta$. Here, again choosing a trial value for $p_c$, one plots the graph of $\gamma$ as a function of $\Delta$. And one looks again for the triplets $(p_c,\gamma,\Delta)$ for which the selected approximants converge to the same point. We give the result for the same trial $p_c=0.2778$ in Fig. 10(b).

The Padé approximants overlap in the boxed area of the Fig. 10(b):

$$1.75<\gamma<1.95 \quad \text{and} \quad 0.95<\Delta<1.05 \ .$$

The determination of $\Delta$ has been sharpened at the expense of that of $\gamma$, which is much larger than above, a fact which weakens somewhat the pertinence and the interest of our findings. To the most commonly accepted value for $\gamma(1.80)$ corresponds here a value of $\Delta$ roughly equal to unity.

The present result can therefore be viewed as consistent with the findings of previous work on other 3D percolation series[37] stating that there is no noticeable confluent singularity for 3D percolation, whereas it seems now established that there is one in 2D.

## APPENDIX D: HIGHER-ORDER MOMENTS OF $n(s)$ AND DETERMINATION OF THE CORRESPONDING EXPONENT $\gamma_k(p)$

The divergence of the $k$th moment of the cluster density function $n(s)$ ($k=3-6$) has been analyzed with the same procedure as that used for $S(p)$ or $P(p)$. Plotting the residue versus the value of the pole yields a cloud of data points, which, curiously, is always pinched in the range (0.25,0.30), in such a way that a single exponential curve can fairly well account for the results in this restricted range at the expense of a reasonable scattering.

The result of the exponential fit is shown in Fig. 11. We excluded from the fit the poles given by the lower-order approximants with $l+m\leq 10$, which yield values departing systematically from the others.

The resulting expressions are found to be

$$\gamma_3(p)=1.908\times 10^{-3}\exp(27.532p) \ ,$$

$$\gamma_4(p)=8.483\times 10^{-3}\exp(23.723p) \ ,$$

$$\gamma_5(p)=2.351\times 10^{-2}\exp(21.173p) \ ,$$

$$\gamma_6(p)=1.051\times 10^{-1}\exp(16.563p) \ .$$

The number of available points in this range drops when the order of the moment increases. For $k=7$, it falls down to 6; although the fititng is still possible over the restricted range, it becomes more and more artificial in view of the remaining data. Note the linear scale for the ordinate axis, which enlightens the fairly constant upward shift for the successive curves at the threshold (roughly positioned at 0.278): The magnitude of the shift is indeed equal to the gap exponent $\beta+\gamma$.

[1]B. J. Last and D. J. Thouless, Phys. Rev. Lett. **27**, 1719 (1971).
[2]S. Kirkpatrick, Phys. Rev. Lett. **27**, 1722 (1971).
[3]S. Kirkpatrick, Rev. Mod. Phys. **45**, 574 (1973).
[4]D. Stauffer, Phys. Rep. **54**, 1 (1979).
[5]D. J. Bergman, Physica A **157**, 72 (1989).
[6]V. Ambegaokar, C. Cochran, and J. Kurkijärvi, Phys. Rev. B **8**, 3682 (1973).
[7]J. A. McInnes and P. N. Butcher, Philos. Mag. B **39**, 1 (1979).
[8]A. Coniglio, J. Phys. A **8**, 1773 (1975).
[9]A. Coniglio and L. Russo, J. Phys. A **12**, 545 (1979).
[10]F. Sevsek, J. M. Debierre, and L. Turban, J. Phys. A **16**, 801 (1983).
[11]S. P. Obukhov, Physica **101A**, 145 (1980).
[12]S. Redner, Phys. Rev. B **25**, 3242 (1982).
[13]D. Wilkinson, J. S. Langer, and P. N. Sen, Phys. Rev. B **28**, 1081 (1983).
[14]V. Halpern, Philos. Mag. B **56**, 861 (1987).
[15]S. Redner and A. C. Brown, J. Phys. A **14**, L285 (1981).
[16]A. Benguigui, Philos. Mag. B **56**, 771 (1987).
[17]R. Landauer, J. Appl. Phys. **23**, 779 (1952).
[18]J. Bernasconi and H. J. Wiesmann, Phys. Rev. B **13**, 1131 (1976).
[19]L. Turban, J. Phys. C **11**, 449 (1978).
[20]J. Bernasconi, Phys. Rev. B **18**, 2185 (1978).
[21]P. J. Reynolds, H. E. Stanley, and W. Klein, Phys. Rev. B **21**, 1223 (1980).
[22]M. H. Ernst and P. F. J. van Velthoven, J. Stat. Phys. **45**, 1001 (1986).
[23]J. P. Straley, Phys. Rev. B **41**, 9340 (1990).
[24]J. R. Manning, in *Diffusion Kinetics of Atoms in Crystals* (Van Nostrand, Princeton, 1968).
[25]P. C. W. Holdsworth and R. J. Elliott, Philos. Mag. A **54**, 601 (1986).
[26]J. L. Bocquet, Acta Metall. **34**, 571 (1986).
[27]J. L. Bocquet, Res. Mech. **22**, 1 (1987).
[28]H. J. de Bruin, G. E. Murch, H. Bakker, and L. P. van der Mey, Thin Solid Films **25**, 47 (1975).
[29]H. J. de Bruin, G. E. Murch, H. Bakker, and L. P. van der Mey, Phys. Status Solidi B **82**, 581 (1977).
[30]H. E. Stanley, J. Phys. A **12**, L329 (1979).
[31]J. L. Martin, in *Phase Transitions and Critical Phenomena,* edited by C. Domb and M. S. Green (Academic, New York, 1972), Vol. 3, p. 97.
[32]S. Redner, J. Stat. Phys. **29**, 309 (1982).
[33]M. F. Sykes and M. Glen, J. Phys. A **9**, 87 (1976).
[34]S. Mertens, J. Stat. Phys. **58**, 1095 (1990).
[35]M. F. Sykes, D. S. Gaunt, and M. Glen, J. Phys. A **9**, 715 (1976).
[36]J. Zinn-Justin, J. Phys. (Paris) **40**, 969 (1979).
[37]J. Adler, Y. Meir, A. Aharony, and A. B. Harris, Phys. Rev. B **41**, 9183 (1990).
[38]R. Z. Roskies, Phys. Rev. B **24**, 5305 (1981).
[39]R.M. Ziff and G. Stell (unpublished).
[40]J. Adler, M. Moshe, and V. Privman, Phys. Rev. B **26**, 1411 (1982).
[41]G. E. Murch and S. J. Rothman, Philos. Mag. A **43**, 229 (1981).